Materials Research Express



RECEIVED

6 June 2019

REVISED

1 September 2019

ACCEPTED FOR PUBLICATION 16 September 2019

PUBLISHED

27 September 2019

PAPER

Large electronic wave function extension of the oxygen vacancies on EuO_{1-x} surface

Aaron Wang¹, Gaurab Rimal², Yuri Dahnovsky, Jinke Tang and TeYu Chien¹

Department of Physics & Astronomy, University of Wyoming, Laramie WY, 82071, United States of America

- ¹ Authors to whom any correspondence should be addressed.
- ² Current address: Department of Physics and Astronomy, Rutgers University, Piscataway, NJ 08904.

E-mail: swang9@uwyo.edu and tchien@uwyo.edu

Keywords: magnetic polaron, surface physics, oxygen vacancies, EuO, scanning tunneling microscopy, density of states, wave function extension

Abstract

EuO $_{1-x}$ thin films deposited by pulsed laser deposition on Si(100) surface is studied by scanning tunneling microscopy and spectroscopy at room temperature. Oxygen vacancies in EuO $_{1-x}$ are visualized through dI/dV mapping and large apparent size of the oxygen vacancies (1.8 nm \pm 0.5 nm) are found, which is in favor of the bound magnetic polaron (BMP) model. These apparent sizes are considered as the spatial extension of the electron wave function originating from the oxygen vacancies. It is further argued that this observed electronic wave function might be the precursor of the BMP formation occurring at lower temperatures. Moreover, some of the oxygen vacancies have been found (1) migrating; (2) appearing; and (3) disappearing, indicating the instability of the oxygen vacancies on the EuO surface at room temperature.

1. Introduction

EuO crystal is a model Heisenberg ferromagnetic semiconductor that draws attentions due to its unique electronic structure and potential spintronic applications [1, 2]. EuO has a Curie temperature of 69 K [3], a bandgap of 1.12 eV [4], and shows colossal magnetoresistance [5], photoconductivity [6], as well as large magneto-optical effects [7, 8]. In the ferromagnetic phase (<69 K), the $4f^7$ electron configuration of Eu²⁺ ion induces a magnetic moment of \sim 7 μ_B (6.9 \pm 0.3 μ_B [9]; or 6.96 \pm 0.07 μ_B [10]) per Eu atom. In the last couple of decades, research on EuO has mostly focused on spintronics applications [11–16]. Owing to the large exchange splitting of 0.6 eV at the bottom of the conduction band [4, 17], a near-fully spin-polarized spin-filter tunneling current [18, 19] is expected. The successful integration of EuO thin films with Si, GaN, and graphene has made it very promising for spintronic applications [11, 20–22].

More interesting phenomena emerge by doping EuO with (i) rare earth elements, La [21, 23–25], Ce [26], Gd [4, 24, 25, 27–34], Sm [27], Ho [25], Y [25], and Lu [35]; (ii) transition metal elements, Fe [36–38], Ag [39], Cu [39], and Eu itself (equivalently, creating oxygen vacancies) [39]; or (iii) oxygen vacancies [27, 29, 34, 40]. For example, a metal-insulator transition occurs with the conductivity increasing by 8–13 orders of magnitude [17, 41–44] upon cooling across the first Curie temperature (69 K). Colossal magnetoresistance [5] and enhancement of the Curie temperature, T_C , to 140–150 K have been observed in EuO_{1-x} samples [27, 29, 34, 40] where the characteristic 'double-dome' M-T curves form. Even higher Curie temperatures (170–200 K) have been reported in rare earth doped EuO samples [23, 32].

Despite the long history of research, the fundamental origin of the intriguing properties of EuO is still controversial. Among various models [23, 41, 45–48], the bound magnetic polaron (BMP) [41], Ruderman-Kittel-Kasuya-Yoshida (RKKY) [23, 48], and ferromagnetic Kondo-lattice model (FKLM) [47] are the most plausible mechanisms describing the enhanced $T_{\rm C}$ in EuO. One of the major distinguishing features across these models is the spatial extension of the electron wave function near the oxygen vacancies or doping impurities. In particular, in the BMP and related models, each oxygen vacancy donates two electrons where one is tightly

bound, while the other is loosely bound. The loosely bound electron is attracted to the oxygen vacancy due to Coulomb interaction resulting in a large Bohr radius, which manifests as a large spatial extension of the electron wave function (\sim nm). This loosely bound electron with large Bohr radius is also in charge of the formation of BMP at lower temperatures [41]. On the other hand, in the RKKY model, the magnetic interactions between Eu²+ are mediated through the conduction electrons; and in the FKLM, the intra-atomic exchange interactions between the localized Eu²+ moments and the conduction electrons are in charge of the electronic properties of the materials. In both the RKKY and FKLM models, the loosely bound electrons from the dopants join the longrange conduction band of the EuO to influence the interactions. In other words, Coulomb interactions do not localize the electron near the vacancies, hence there is no spatial extension of the electron wave function near the oxygen vacancies is expected. This effect can be considered as a point defect with an apparent size in the order of Å when measured by scanning tunneling microscopy (STM). Thus, by measuring the apparent sizes of the oxygen vacancies, the favorable model can be determined. In this research spatial extension of the electron wave function centered at the oxygen vacancies on EuO $_{1-x}$ surfaces is revealed by using scanning tunneling microscopy and spectroscopy (STM/S). We find that the large oxygen vacancy apparent size is in favor of the BMP picture.

2. Experimental methods

EuO $_{1-x}$ was deposited on Si(100) substrate by pulsed laser deposition (PLD). The target was Eu (99.9%) metal target purchased from Alfa Aesar. The substrate was cleaned with deionized water and isopropyl alcohol (IPA) before loading into the PLD chamber. The substrate was heated to 340 °C and kept for 1 h prior to the deposition. The base pressure in the chamber was about 4×10^{-8} mbar. Because Eu can be easily over-oxidized into Eu $_2$ O $_3$ or Eu $_3$ O $_4$, no extra oxygen was leaked into the high vacuum system and the EuO $_{1-x}$ growth relied only on the residual oxygen in the system. The film was deposited using a laser fluence of 320 mJ/pulse with the repetition rate of 10 Hz, using a LOTIS TII Nd:YAG pulsed laser at fourth harmonic (266 nm). The film was capped with a thin layer of Pt *in-situ* to avoid further oxidation of the films during the transfer to the chamber for STM/S measurements. The phase and crystallinity of the deposited films were investigated *ex-situ* using X-ray diffraction (XRD) with Cu- K_{α} radiation.

Prior to the STM/S measurements, the Pt capping layers were removed by Ar $^+$ -ion sputtering at a pressure of 5×10^{-5} mbar for $30 \, \text{min}$ ($V = 3 \, \text{kV}$, $I_{\text{emission}} = 5 \, \text{mA}$, $I_{\text{sample}} = 1 \, \mu \text{A}$) with the incident angle of 45° followed by a 30-min annealing process at $300\,^\circ\text{C}$ with a base pressure of 5×10^{-10} mbar or better. The annealing process in the ultra-high vacuum (UHV) environment also served the purpose of inducing a low level of oxygen vacancies. STM/S measurements were conducted at room temperature with a base pressure of 1×10^{-11} mbar. Electronic local density of states (LDOS) information was revealed by the dI/dV measurement with lock-in technique. The modulation frequency of the lock-in amplifier for all spectroscopic data was set to 2 kHz and the time constant to 1 ms. The dI/dV images were taken simultaneously with the topography images. Each image has a resolution of 450×450 pixels and each pixel scanning time is $2.2 \, \text{ms}$. Thus, the measurement time for each image is $14 \, \text{min} 51 \, \text{s}$. All the dI/dV spectra were measured in a bias range from $-3.3 \, \text{V}$ to $+3.5 \, \text{V}$ with $500 \, \text{data}$ points while each point with $90 \, \text{ms}$ of measurement time. Each dI/dV point spectrum was repeated 3 times for repeatability check. The spectra shown in figure 2(a) were averaged over the three consecutive and consistent measurements. The set point bias was $-3.3 \, \text{V}$ and the set tunneling current was $200 \, \text{pA}$ for the dI/dV spectrum measurements. The thermal drift for the scan was determined by consecutive images and found to be $\sim 0.2 \, \text{Å} \, \text{min}^{-1}$.

3. Results and discussions

Figure 1(a) shows the XRD data of the Pt/EuO/Si(100) taken prior to the STM measurements. A strong EuO (111) peak located at 29.644 \pm 0.005° is revealed, corresponding to the EuO lattice constant of 5.22 \pm 0.05 Å, which is close to the previously reported value, 5.141 Å [2, 49]. Pt(111) is also visible at 39.91 \pm 0.01° since it is not removed yet during the XRD measurements. The thickness of the EuO film is around 30 nm, calibrated by samples deposited with similar conditions. Prior to the STM measurements, the Pt capping layer was removed by *in-situ* sputtering/annealing procedures in UHV environment as described in the experimental methods section.

Figure 1(b) shows the dI/dV mapping of the EuO_{1-x} surfaces measured with tip-sample bias of -3.3 V. Scattered dot-like features are observed and are likely to be related to the oxygen-vacancy-induced changes in the electronic LDOS. The density of the oxygen vacancies is determined to be $0.005/\mathrm{nm}^2$, which corresponds to 0.06% of oxygen vacancies per pristine surface primitive cell. This amount is considered as a lightly oxygen deficient EuO_{1-x} . In order to confirm that the dot-like features are indeed associated with the oxygen vacancies,

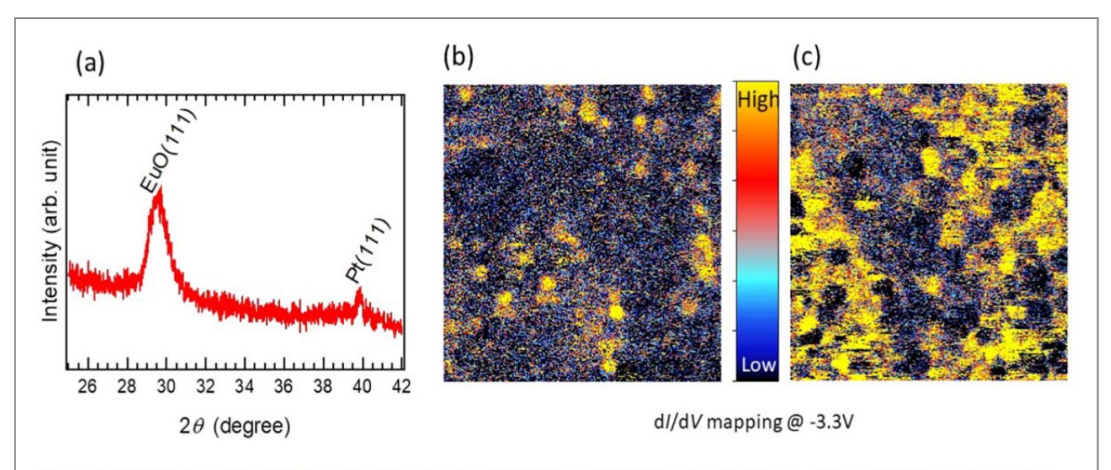


Figure 1. (a) XRD data of the PLD deposited film showing EuO(111) and Pt(111) peaks. (b) $40 \text{ nm} \times 40 \text{ nm} \, \text{d} I / \text{d} V$ mapping on the EuO_{1-x} surfaces after sputtering and 300 °C annealing. (c) $40 \text{ nm} \times 40 \text{ nm} \, \text{d} I / \text{d} V$ mapping on the EuO_{1-x} surfaces after an extra annealing for 30 min at 500 °C.

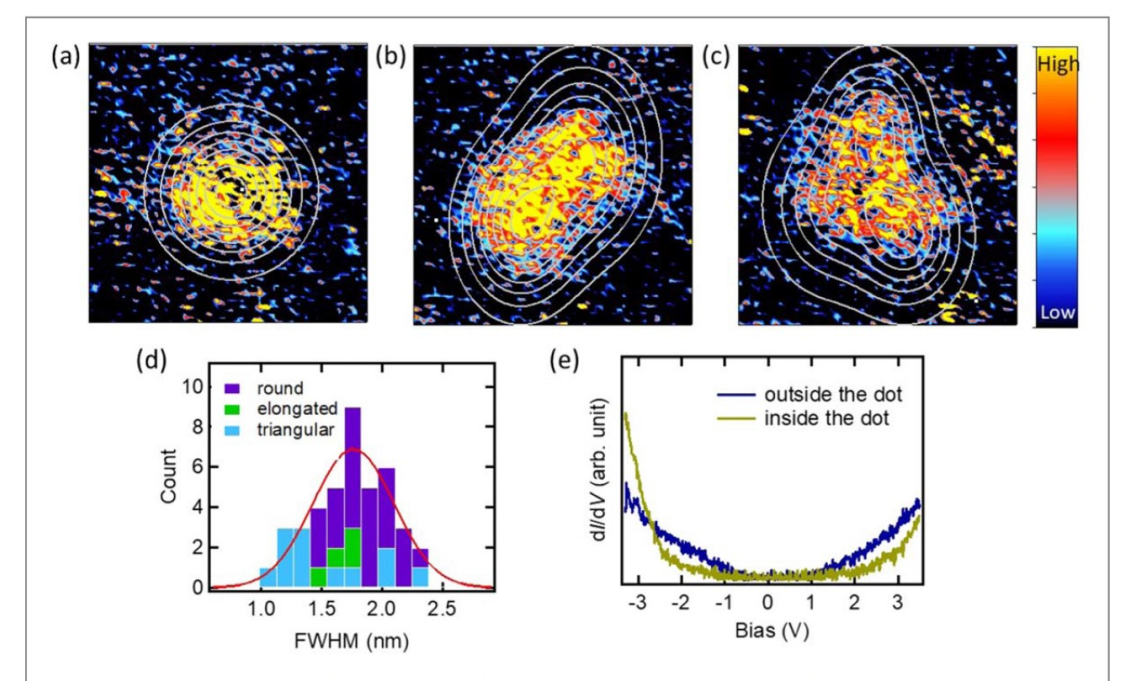


Figure 2. 5 nm \times 5 nm dI/dV mappings measured on the 300 °C-annealed samples. Three types of features along with the fitting contour plot are: (a) Round shaped dot; (b) Elongated dot; and (c) Triangular dot. (d) Histogram of the extracted dot diameters along with a Gaussian function fitting (red curve). Different colors of the bars represent data points from different types of dots (purple for round shaped, green for elongated, and blue for triangular) (e) dI/dV spectra measured inside (dark gold) and outside (dark blue) of the dot-like regions.

extra annealing at $500\,^{\circ}$ C for 30 min in UHV is performed and the result is shown in figure 1(c). It is clear that the number of dot-like features increases, overlaps with neighboring dots. It is known that the oxygen vacancy concentrations in oxides could be controlled by annealing process under oxygen-poor or oxygen-rich environment [50–52]. Hence, it is expected that the annealing procedure in UHV creates more oxygen vacancies, hence the increased density of the dots.

The dI/dV spectra taken inside and outside of the dots are shown in figure 2(e). The spectra clearly indicate that the band gap outside the dot is smaller than that inside. Also, the spectral weight of the electronic LDOS between the two vary. Specifically, from the outside to the inside of the dot, the dI/dV signal near the Fermi energy decreases accompanied by the increase of the dI/dV signal at higher binding energies.

Now, we focus on the apparent sizes of the oxygen vacancies. First, it is obvious that the apparent sizes of the dots are of the nm scale. Since the dI/dV signals are closely related to the electronic LDOS, the apparent sizes in dI/dV mappings can be used to describe the spatial extension of the electron wave functions associated with the

oxygen vacancies. By inspecting the individual dots from the 300 $^{\circ}$ C-annealed samples, three dot shapes are classified: (1) round shaped; (2) elongated; and (3) triangular, as shown in figures 2(a)–(c). Note that the images measured on the 500 $^{\circ}$ C annealed samples are not feasible for the size analysis due to the overlapping of the dot features. It is clear that the elongated dots are larger than the round shaped dots; and the triangular dots are typically larger than the elongated dots. This observation indicates that the elongated dots and the triangular dots are possibly composed of two and three nearby oxygen vacancies, respectively. The diameters of the round shaped dots (figure 2(a) type) are extracted by fitting the dI/dV mappings with an isotropic two-dimensional Gaussian function:

$$f(x, y) = z + Ae^{\frac{-(x-x_0)^2 + (y-y_0)^2}{2c^2}}$$
 (1)

where z is the background of the dI/dV image, A is the amplitude, x_0 and y_0 denote the position of the center of the dot. The diameters of the dots are quoted to be the FWHM of the fitting. It is given as: $FWHM = 2\sqrt{2 \ln 2} c$, where c is a fitting parameter in equation (1). Note that throughout the paper, 'sizes' of the dot features are referring to the FWHM (or the diameter) of the dI/dV images. The fitting results for a round shaped dot is shown as the contour plot in figure 2(a). The round shaped dots have an average size of 1.8 nm \pm 0.2 nm. This size is the spatial range of the affected LDOS on EuO surface due to a single oxygen vacancy.

The elongated dots and triangular dots are formed by two and three neighboring oxygen vacancies, respectively. The fitting of these features is done with two and three Gaussian functions with independent amplitude *A* and dot size parameters *c* as:

$$f(x, y) = z + A_1 e^{\frac{-(x-x_1)^2 + (y-y_1)^2}{2c_1^2}} + A_2 e^{\frac{-(x-x_2)^2 + (y-y_2)^2}{2c_2^2}}$$
(Elongated dots) (2)

$$f(x, y) = z + A_1 e^{\frac{-(x-x_1)^2 + (y-y_1)^2}{2c_1^2}} + A_2 e^{\frac{-(x-x_2)^2 + (y-y_2)^2}{2c_2^2}} + A_3 e^{\frac{-(x-x_3)^2 + (y-y_3)^2}{2c_3^2}}$$
(Triangular dots) (3)

Figures 2(b) and (c) show the fitting results. It is found that the sizes extracted from the three types of dot features are within the error bars (round shaped 1.8 nm \pm 0.2 nm, elongated 1.6 nm \pm 0.1 nm, and triangular 1.5 nm \pm 0.4 nm). The statistics of the size information from the 41 oxygen vacancies found in a series of 80 nm \times 80 nm and 28 nm \times 28 nm dI/dV mappings is analyzed and shown as the histograin figure 2(d). The size information acquired from three different types of dots is grouped with different colors: purple (round shaped), green (elongated), and blue (triangular). The consistent size among the three different types confirm that the elongated and triangular features originate from the nearby two and three oxygen vacancies, respectively. The overall size distribution when considering all three types is 1.8 nm \pm 0.5 nm, by fitting the combined histogram (figure 2(d)) with a Gaussian normal distribution function.

There are related topography changes located at the dots in the dI/dV, as demonstrated in figures 3(a) and (b). At the locations where there is high contrast (dots) in the dI/dV mapping (see figure 3(a)), the topography exhibits the small dot-like features as well (see figure 3(b)). This can be seen more obviously with the line profiles shown in figures 3(c) and (d). The double protrusion in the dI/dV mappings has the same location where the similar topography features are observed. The height of the observed topography is determined to be about 1 Å. This small apparent height at the location of the oxygen vacancy is a result of the combination of a missing oxygen atom (real topography change) as well as a higher dI/dV signal (electronic change).

The previous STM studies on EuO surface also confirm that the apparent diameters of the oxygen vacancies in topography images are about 1 nm at 5.3 K [22] and 1–2 nm at room temperature [53]. However, neither statistical analysis, nor detailed discussions were provided in those studies. On the other hand, from an ARPES data on $Eu_{1-x}Gd_xO$, it was estimated that the real space FWHM of the defect wave function extension is about 1 nm at temperature of 140 K [54]. As pointed out, the Ce [26] and Gd [29] doped EuO exhibit different behaviors in the magnetic properties compare to that of the oxygen deficient EuO_{1-x} . Thus, the wave function extensions in both cases do not necessarily have the same sizes. It is interesting to see that the Gd dopant showed similar spatial size in electron wave function compared to that of the oxygen vacancies in EuO_{1-x} observed here. Overall, the apparent sizes of the oxygen vacancy electron wave function analyzed here agree well with the previous studies. The main difference is that, instead of topography, our oxygen vacancies data were acquired through dI/dV mapping, which is closely related to the electronic LDOS. In addition, in this work, detailed analysis and statistics are provided for the spatial extension size of the oxygen vacancy induced wave function.

It is worth noting that the large spatial extension of the defect electron wave function observed here is uncommon in oxides. For examples, STM measurements revealed that the apparent size of the oxygen vacancies are around a single atomic site on TiO_2 rutile (110) [55] and TiO_2 anatase (101) [56]; while that on $PrSr_2Mn_2O_7$ are slightly less than 1 nm [57]. On the other hand, large defect wave function extension has been observed in semiconductors, such as Si substitution defect in β —. Ga_2O_3 , where the electron wave function extension is reported to be ~2.4 nm (visualized with STM) [58], and ~2 nm (estimated from ARPES measurements) [59] in

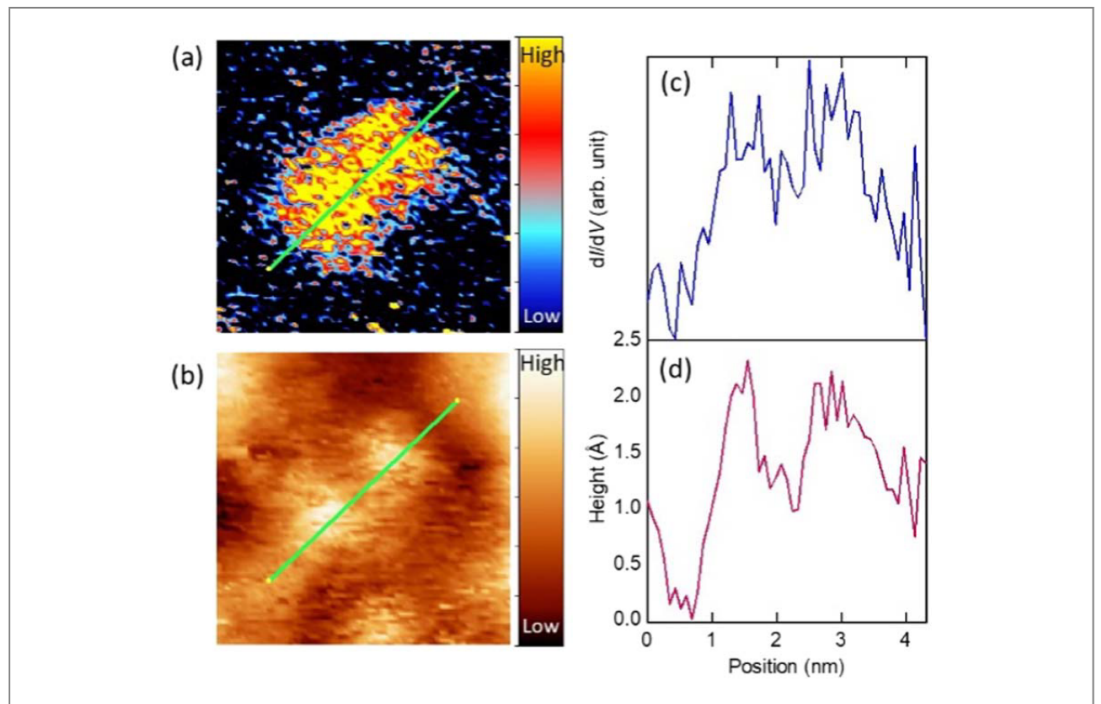


Figure 3. (a) $5 \text{ nm} \times 5 \text{ nm} \text{ d}I/\text{d}V$ mappings and (b) topography image from 300 °C-annealed sample. (c), (d) line profiles extracted from the green line region in (a) and (b), respectively.

diameter; while Mn dopant in GaAs shows \sim 2 nm apparent diameters [60, 61]. The large spatial extension of the electron wave function in EuO_{1-x} is explained with the Bohr's model, a precursor model for the BMP model.

According to Liu *et al.* [62], the oxygen vacancies become the centers of the BMPs. It was assumed that the size of the BMP is similar to the Bohr radius [63, 64], which was used as a means of estimating the size of BMP [62]. With this very simple model, the Bohr radius of the loosely bound electrons near the oxygen vacancies was estimated by $a_0 = \kappa_0 \frac{\hbar^2}{m^* e^2}$. With the dielectric constant $\kappa_0 = 23.9$, and a range of the reported effective mass of $m^* = 0.35 m_e$ [4]; $0.42 m_e$ [65]; $0.52 m_e$ [66]; and $1.1 m_e$ [67], the Bohr radius is estimated to be in the range of 1.2–3.6 nm. To directly compare to the estimated sizes with that found from the STM/S measurements, we determine the FWHM of the electron density from the wave function. According to the hydrogen atom model, an electron wave function of the ground state can be written as $\psi(r) = \frac{1}{\sqrt{\pi}} \left(\frac{1}{a_0}\right)^{3/2} e^{-r/a_0}$. Thus, the electron density can be expressed as the square of the absolute value of the wave function as:

Election Density =
$$|\psi(r)|^2 = \frac{1}{\pi} \left(\frac{1}{a_0}\right)^3 e^{-r/\left(\frac{a_0}{2}\right)}$$
 (4)

Using the estimated a_0 (1.2–3.6 nm), the FWHM radius can be obtained from the following equation:

$$\frac{|\psi(r = FWHM)|^2}{|\psi(r = 0)|^2} = \frac{1}{2} = e^{-r_{FWHM}/\left(\frac{a_0}{2}\right)}$$
 (5)

From this equation, $r_{FWHM} = \frac{-a_0}{2} \ln \left(\frac{1}{2} \right) = 0.42 \text{ nm} - 1.25 \text{ nm}$. Thus, the FWHM (the diameter) of the BMP is estimated to be 0.82 nm - 2.5 nm (average value of $1.7 \text{ nm} \pm 0.8 \text{ nm}$). This is consistent with the experimental values determined from STM measurements: $1.8 \text{ nm} \pm 0.5 \text{ nm}$. With these results, the large spatial extension of the wave function is in favor of the BMP model. The unusually large electron wave function radius might be unique to EuO case. It is due to the combination of the high dielectric constant, the small electron effective masses and the working mechanism needs to be the BMP model.

Finally, it is worth to mention that during the measurements, it has been noticed that nine out of the forty-one measured dots are not stable over the time scale of tens of minutes. Some dots were found (a) appear; (b) migrate; or (c) disappear, compare to a prior scan, as illustrated in figure 4. In figures 4(a) and (b) the dot at the top-right corner appears in one image compare with previous image taken \sim 40 min earlier. In figures 4(c) and (d) near the bottom-right corner, a dot moves \sim 1 nm in \sim 9 min And in figures 4(e) and (f), the dot at the right disappears 40 min later. These images clearly show that some of the oxygen vacancies near the surface are unstable. However, with the long scanning time (\sim 15 min per image), it is impossible to extract the activation

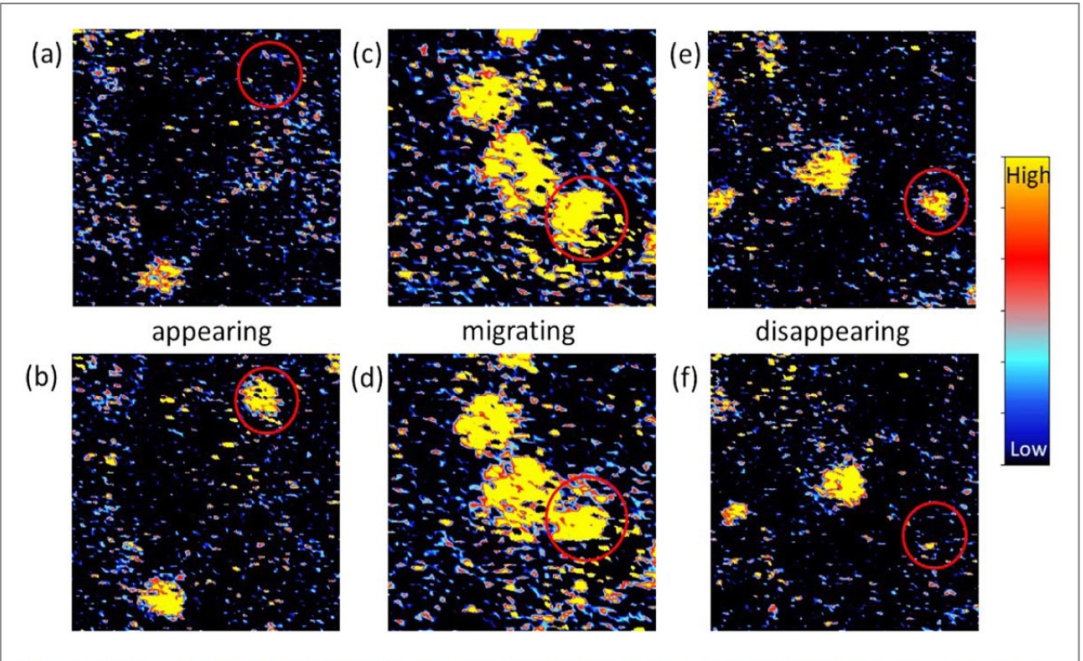


Figure 4. 20 nm \times 20 nm dI/dV mappings of the consecutive scanning of the three types of unstable events of the oxygen vacancies: (a), (b) appearing; (c), (d) migrating; and (e), (f) disappearing.

energy for this instability. Further experiments are needed to understand the origin of the instability. Similar behavior was also found in a previous experiment for an anatase $TiO_2(010)$ surface [68].

4. Conclusion

In conclusion, we present the STM/S measurements on PLD prepared EuO thin films at room temperature. Oxygen vacancies are visualized in the dI/dV mappings where the large portion of them is distributed sparsely and isolated with a low oxygen vacancy density. The apparent sizes of the oxygen vacancies are determined to be $1.8~\rm nm\,\pm\,0.5~\rm nm$. The observed large apparent size of the oxygen vacancy is associated with the large spatial extension of the electronic wave function, which is explained with Bohr model. These results are in favor of the BMP model in EuO and ruling out RKKY and FKLM models. Moreover, the stability of the oxygen vacancies is studied. In particular, their appearance, migration and disappearance are all observed on the EuO $_{1-x}$ surface. The information present here is helpful to further study the magnetic polarons in EuO.

Acknowledgments

This work is financially supported by the U S National Science Foundation, Division of Materials Research (DMR) (Grants No. DMR-1710512).

Author contribution

A. W. performed the STM experiment and analyzed the XRD and STM data. G. R. prepared the samples with the PLD and performed the XRD experiments. All authors contributed to the writing of the manuscript.

ORCID iDs

Aaron Wang https://orcid.org/0000-0002-2652-3876

References

- [1] Mauger A and Godart C 1986 Phys. Rep. 141 51
- [2] Matthias BT, Bozorth RM and Vleck JH V 1961 Phys. Rev. Lett. 7 160 $\,$
- [3] Kornblit A and Ahlers G 1975 Phys. Rev. B 11 2678

- [4] Schoenes J and Wachter P 1974 Phys. Rev. B 9 3097
- [5] Shapira Y, Foner S and Reed T B 1973 Phys. Rev. B 8 2299
- [6] Bachmann R and Wachter P 1968 Solid State Commun. 6711
- [7] Greiner J H and Fan G J 1966 Appl. Phys. Lett. 9 27
- [8] Suits J C and Lee K 1971 J. Appl. Phys. 42 3258
- [9] Iwata N, Pindoria G, Morishita T and Kohn K 2000 J. Phys. Soc. Japan 69 230
- [10] Ulbricht RW, Schmehl A, Heeg T, Schubert J and Schlom D G 2008 Appl. Phys. Lett. 93 102105
- [11] Lev L L, Averyanov D V, Tokmachev A M, Bisti F, Rogalev V A, Strocov V N and Storchak V G 2017 J. Mater. Chem. C 5 192
- [12] Gerber T, Lömker P, Zijlstra B, Besson C, Mueller D, Zander W, Schubert J, Gorgoi M and Müller M 2016 J. Mater. Chem. C 4 1813
- [13] Prinz GM, Gerber T, Lorke A and Müller M 2016 Appl. Phys. Lett. 109 202401
- [14] Pradip R et al 2016 Phys. Rev. Lett. 116 185501
- [15] Ohuchi Y, Kozuka Y, Uchida M, Ueno K, Tsukazaki A and Kawasaki M 2015 Phys. Rev. B 91 245115
- [16] Mairoser T et al 2015 Nat. Commun. 6 7716
- [17] Steeneken P G, Tjeng L H, Elfimov I, Sawatzky G A, Tjeng L H, Ghiringhelli G, Brookes N B and Huang D-J 2002 Phys. Rev. Lett. 88 047201
- [18] Santos T S, Moodera J S, Raman K V, Negusse E, Holroyd J, Dvorak J, Liberati M, Idzerda Y U and Arenholz E 2008 Phys. Rev. Lett. 101 147201
- [19] Müller M, Miao G-X and Moodera J S 2009 Europhys. Lett. 88 47006
- [20] Averyanov DV, Sadofyev YG, Tokmachev AM, Primenko AE, Likhachev IA and Storchak VG 2015 ACS Appl. Mater. Interfaces 76146
- [21] Schmehl A et al 2007 Nat. Mater. 6 882
- [22] Klinkhammer J, Schlipf M, Craes F, Runte S, Michely T and Busse C 2014 Phys. Rev. Lett. 112 016803
- [23] Miyazaki H, Im H J, Terashima K, Yagi S, Kato M, Soda K, Ito T and Kimura S 2010 Appl. Phys. Lett. 96 232503
- [24] Ahn KY and McGuire TR 1968 J. Appl. Phys. 39 5061
- [25] Shafer MW and McGuire TR 1968 J. Appl. Phys. 39 588
- [26] Liu P, Tang J, Colón Santana J A, Belashchenko K D and Dowben P A 2011 J. Appl. Phys. 109 07C311
- [27] Borukhovich A S, Bamburov V G and Sidorov A A 1988 J. Magn. Magn. Mater. 73 106
- [28] Mairoser T et al 2011 Appl. Phys. Lett. 98 102110
- [29] Wang X, Liu P, Fox K A, Tang J, Colón Santana J A, Belashchenko K, Dowben P A and Sui Y 2010 IEEE Trans. Magn. 46 1879
- [30] Mairoser T et al 2010 Phys. Rev. Lett. 105 257206
- [31] Sutarto R et al 2009 Phys. Rev. B 80 085308
- [32] Ott H, Heise SJ, Sutarto R, Hu Z, Chang cf, Hsieh HH, Lin H-J, Chen CT and Tjeng LH 2006 Phys. Rev. B 73 094407
- [33] Von Molnar S and Shafer M W 1970 J. Appl. Phys. 41 1093
- [34] Matsumoto T, Yamaguchi K, Yuri M, Kawaguchi K, Koshizaki N and Yamada K 2004 J. Phys. Condens. Matter 16 6017
- [35] Melville A et al 2012 Appl. Phys. Lett. 100 222101
- [36] Ahn KY 1970 Appl. Phys. Lett. 17 347
- [37] Ahn KY, Tu K N and Reuter W 1971 J. Appl. Phys. 42 1769
- [38] McGuire TR, Petrich GF, Olson BL, Moruzzi VL and Ahn KY 1971 J. Appl. Phys. 42 1775
- [39] Lee K and Suits J C 1971 Phys. Lett. A 34A 141
- [40] Massenet O, Capiomont Y and Van Dang N 1974 J. Appl. Phys. 45 3593
- [41] Torrance J B, Shafer M W and McGuire T R 1972 Phys. Rev. Lett. 29 1168
- [42] Oliver M R, Kafalas J A, Dimmock J O and Reed T B 1970 Phys. Rev. Lett. 24 1064
- [43] Oliver MR, Dimmock JO, Mcwhorter AL and Reed TB 1972 Phys. Rev. B5 1078
- [44] Penney T, Shafer M W and Torrance J B 1972 Phys. Rev. B 5 3669
- [45] Arnold M and Kroha J 2008 Phys. Rev. Lett. 100 046404
- [46] Sinjukow P and Nolting W 2003 Phys. Rev. B 68 125107
- [47] Schiller R, Müller W and Nolting W 2001 Phys. Rev. B 64 134409
- [48] Monteiro P M S, Baker P J, Ionescu A, Barnes C H W, Salman Z, Suter A, Prokscha T and Langridge S 2013 Phys. Rev. Lett. 110 217208
- [49] Ahn K Y and Shafer M W 1970 J. Appl. Phys. 41 1260
- [50] Muller D A, Nakagawa N, Ohtomo A, Grazul J L and Hwang HY 2004 Nature 430 657
- [51] Kalabukhov A, Gunnarsson R, Börjesson J, Olsson E, Claeson T and Winkler D 2007 Phys. Rev. B 75 121404
- [52] Iijima K, Goto M, Enomoto S, Kunugita H, Ema K, Tsukamoto M, Ichikawa N and Sakama H 2008 J. Lumin. 128 911
- [53] Förster D F, Klinkhammer J, Busse C, Altendorf S G, Michely T, Hu Z, Chin Y-Y, Tjeng L H, Coraux J and Bourgault D 2011 Phys. Rev. B 83 045424
- [54] Shai D E, Fischer M H, Melville A J, Monkman E J, Harter J W, Shen D W, Schlom D G, Lawler M J, Kim E-A and Shen K M 2016 Phys. Rev. B 94 195102
- [55] Wahlström E, Lopez N, Schaub R, Thostrup P, Rønnau A, Africh C, Laegsgaard E, Nørskov J K and Besenbacher F 2003 Phys. Rev. Lett. 90 026101
- [56] Setvin M, Aschauer U, Scheiber P, Li Y-F, Hou W, Schmid M, Selloni A and Diebold U 2013 Science 341 988
- [57] Bryant B, Renner C, Tokunaga Y, Tokura Y and Aeppli G 2011 Nat. Commun. 2 212
- [58] Iwaya K, Shimizu R, Aida H, Hashizume T and Hitosugi T 2011 Appl. Phys. Lett. 98 142116
- [59] Richard P, Sato T, Souma S, Nakayama K, Liu HW, Iwaya K, Hitosugi T, Aida H, Ding H and Takahashi T 2012 Appl. Phys. Lett. 101 232105
- [60] Garleff J K, Çelebi C, Van Roy W, Tang J-M, Flatté M E and Koenraad P M 2008 Phys. Rev. B 78 075313
- [61] Jancu J-M, Girard J-C, Nestoklon MO, Lemaître A, Glas F, Wang ZZ and Voisin P 2008 Phys. Rev. Lett. 101 196801
- [62] Liu P and Tang J 2013 J. Phys. Condens. Matter 25 125802
- [63] Durst A C, Bhatt R N and Wolff P A 2002 Phys. Rev. B 65 235205
- [64] Kuivalainen P, Sinkkonen J and Stubb T 1981 Phys. Status Solidi 104 299
- [65] Patil C G and Krishnamubthy B S 1981 Phys. Status Solidi 105 391
- [66] Mauger A 1983 Phys. Rev. B 27 2308
- [67] Bebenin N G 1985 Solid State Commun. 55 823
- [68] Scheiber P, Fidler M, Dulub O, Schmid M, Diebold U, Hou W, Aschauer U and Selloni A 2012 Phys. Rev. Lett. 109 136103